UNCLASSIFIED

AD 423178

DEFENSE DOCUMENTATION CENTER

FOR

SCIENTIFIC AND TECHNICAL INFORMATION

CAMERON STATION, ALEXANDRIA, VIRGINIA

UNCLASSIFIED

n a b

423178

STUDIES OF MAGNETIC SHIELDING

AND

SUPERCONDUCTIVITY

D D C

NOV 21 1963

TISIA D

GENERAL DYNAMICS | FORT WORTH

GIIIIIIID

STUDIES OF MAGNETIC SHIELDING AND SUPERCONDUCTIVITY

J. M. Norwood
and
F. L. Gibbons

1 August 1963

ENGINEERING DEPARTMENT

GENERAL DYNAMICS | FORT WORTH

ABSTRACT

Theoretical considerations of magnetic (active) shielding of
space vehicles against charged-particle cosmic-radiation indicate
inadequate treatment in feasibility studies. Simplified expres-
sions for the magnetic vector potential lead to predictions of
possibly fictitious completely-shielded regions. The mathematical
model presented herein avoids this deficiency, and a method of
determining the completely shielded regions is developed. Experi-
mental investigations establish the capability of winding super-
conducting solenoids and making junctions between superconducting
wire and current-carrying leads. Junctions made by spot welding
superconducting Nb-Zr wire to copper electrodes, including foil,
prove to be superior in reliability, simplicity, and high current
capacity. Critical currents in three superconducting solenoids,
constructed to operate at 10-, 15-, and 22-kilogauss, were lower
than those measured in short segments by amounts consistent with
data in available literature. Persistent currents were estab-
lished in two of the solenoids.

TABLE OF CONTENTS

1. GENERAL INTRODUCTION

The objective of this investigation is to provide theoretical and experimental analysis pertinent to the utilization of superconducting magnets as shielding systems for the protection of space vehicles against charged-particle radiation. The most dangerous charged-particle radiation for long space flights originates in solar flares and consists for the most part of high-energy protons. Artificial and natural trapped radiation, primary cosmic radiation, and other miscellaneous radiations are of lesser importance, although the analysis is applicable to any energetic charged-particle. Reference 1 contains a comprehensive discussion of space radiation hazards.

Although protons of energies less than 50 to 100 Mev are readily stopped by passive (bulk) shields, the bulk shielding weight required to stop increasingly higher-energy protons and their secondaries becomes excessive. Shielding will probably be required for protection against protons of energies up to 500 Mev or 1 Bev, and it is conceivable that this protection can be accomplished by magnetic shielding systems with weight comparatively less than that of equivalent passive shielding. Magnetic (active) shielding systems necessarily involve superconducting current elements because of weight and power requirements.

Independent investigations were pursued in theory and experiment. The theoretical analysis, accomplished by J. M. Norwood, is recorded in Section 2. The experimental investigation, performed by F. L. Gibbons, is reported in Section 3. Conclusions and recommendations for further work are in Section 4.

2. THEORY OF MAGNETIC SHIELDING

The original aim of the theoretical study was to investigate
the active-passive shielding capabilities of the structural mater-
ial and superconducting coils of active-passive shielding config-
urations; that is, the aim was to study the shielding provided by
the magnetic field and bulk material combined. Past tentative studies
(Refs. 2 and 3) indicate that combined active and passive radiation
shielding offers no significant advantage over passive shielding
alone, but active-passive studies are still of interest because of
the necessary thicknesses of superconducting material and support
structure. Large thicknesses of bulk material may modify and pos-
sibly negate active shielding design.

A study of available active-shielding literature resulted in a
shift of emphasis to more basic studies. Meaningful active-passive
investigations are premature since they should be based upon know-
ledge of realistic shielding geometries and associated magnetic
fields. No such information is available. Active-passive shielding
studies are but one phase of the more general active-shielding design
problem and should be treated as such.

The most prominent investigation of active shielding is that of
Levy (Ref. 4). His analysis predicts a toroidally-shaped completely-
shielded region surrounding a circular current-loop. Accordingly, a
superconducting ring with large diameter or a configuration of such
rings centered on a common axis was chosen for study as a reasonable
field-producing geometry. Configurations of such current rings
centered about a common axis and spaced so that individual completely-

2

shielded regions are contiguous should provide effective active shielding; rings placed on appropriately spaced circles of latitude on a spherical surface, for example, should shield the interior of the sphere (except possibly at the poles).

Levy's analysis, which was only preliminary, was based upon a simplified mathematical model possessing a fictitious infinity which necessarily insures the existence of the toroidally-shaped completely-shielded region. Such infinities do not occur in nature, and under circumstances to be explained the completely shielded region may not exist. More realistic equations have been derived and a method of investigation has been devised which should clarify this problem and should be useful in active-shield design. Active-passive shielding studies can be resumed, if desirable, once realistic active shielding design configurations are obtained.

2.1 Analytical Formulation

The fundamental theory underlying active shielding is due to Störmer and was originally applied to the motion of cosmic rays in the magnetic field of the earth. Since the literature on Stömer's theory is extensive (see for example Ref. 5), the presentation to follow is somewhat brief. An example of Störmer's theory applied to dipole shielding of space vehicles can be found in Reference 6.

The equation which leads to the definition of completely shielded regions (forbidden regions) in Störmer's theory for an arbitrary axially-symmetric magnetic-field is easily derived from the relativistic Lagrangian, which is

$$L = m_o c^2 \left[1 - \sqrt{1-(v/c)^2} \right] + e\vec{v} \cdot \vec{A} \tag{1}$$

3

in which m_0 is the particle rest mass, c the speed of light, e the particle charge, $\vec{v}$ the particle velocity, and $\vec{A}$ the magnetic vector potential. In spherical polar coordinates r, θ, and ϕ

$$v^2 = \dot{r}^2 + r^2 \dot{\theta}^2 + r^2 \dot{\phi}^2 \sin^2\theta \tag{2}$$

where θ is the co-latitude angle and ϕ is the longitude. It can be shown that

$$\vec{v} \cdot \vec{A} = Ar\dot{\phi} \sin\theta \tag{3}$$

since $\vec{A} = 1_\phi A$ in an axially symmetric field. Application of the equation

$$\frac{d}{dt} \frac{\partial L}{\partial \dot{\phi}} - \frac{\partial L}{\partial \phi} = 0 \tag{4}$$

to Equation (1) and subsequent integration over time yields

$$mr^2\dot{\phi}\sin^2\theta + eAr \sin\theta = p \tag{5}$$

where p is an arbitrary constant. Mass m is also constant since v is constant in a magnetic field. In the limit as r approaches infinity, A approaches zero and the first term of Equation (5) approaches p. Thus p is the initial condition at infinity of the component of the angular momentum about the axis of symmetry. In the absence of the magnetic field, a particle from infinity would pass the origin of coordinates at a distance of closest approach b. Hence

$$p = mvb \cos H, \quad -\infty < b < \infty \tag{6}$$

where H is the angle between $\vec{r} \times m\vec{v}$ and the axis of symmetry and is evaluated at $\vec{r} = \vec{b}$ (when $\vec{B} = 0$).

4

The component of $\vec{v}$ in the plane of symmetry of the magnetic field is

$$v_\emptyset = r\dot{\emptyset}\sin\theta \tag{7}$$

so Equation (5) can be written

$$Q = \frac{v_\emptyset}{v} = \frac{b \cos H}{r \sin\theta} - \frac{e}{mv} A \tag{8}$$

where

$$-1 \leq Q \leq 1 \tag{9}$$

With

$$z = r \cos\emptyset \tag{10}$$

$$\rho = r \sin\emptyset \tag{11}$$

the equation for the vector potential of an axially symmetric magnetic field is

$$A(\rho,z) = \frac{\mu_0}{4\pi} \int\limits_{\rho_1}^{\rho_2} \int\limits_{0}^{2\pi} \int\limits_{z_1(\rho')}^{z_2(\rho')} \frac{j(\rho',z')\rho'\cos\emptyset' dz' d\emptyset' d\rho'}{\sqrt{\rho^2 - 2\rho\rho'\cos\emptyset' + \rho'^2 + (z-z')^2}} \tag{12}$$

where ρ, $\emptyset$, and z are cylindrical coordinates and j is current density. MKS units are used.

It is convenient to scale coordinates ρ and z in terms of

$$C = \sqrt{\frac{4\pi}{\mu_0} \frac{m}{e j_s}} \text{ meters} \tag{13}$$

so ρ and z are dimensionless; $C\rho$ and Cz are substituted for ρ and z, and by this means Equation (8) can be made independent of mv. It becomes

$$Q = \frac{\beta}{\rho} - U(\rho,z) \tag{14}$$

with

$$U(\rho,z) = \int_{\rho_1}^{\rho_2} \int_0^{2\pi} \int_{z_1(\rho')}^{z_2(\rho')} \frac{j(\rho',z')}{j_s} \frac{\rho'\cos\phi'\,dz'\,d\phi'\,d\rho'}{\sqrt{\rho^2-2\rho\rho'\cos\phi'+\rho'^2+(z-z')^2}} \quad (15)$$

where now ρ, z, and β replace ρ/C, z/C, and $(b/C)\cos H$, with β arbitrary $(-\infty < \beta < \infty)$; j_s is an arbitrary reference current density. If $j(\rho',z')$ is independent of ρ' and z', and if j_s is set equal to j, Equations (14) and (15) are independent of j in addition to being independent of mv.

It can be shown that $U(\rho,z)$ is finite for all ρ and z, is zero for $\rho = 0$, and

$$\lim_{\rho \to \infty} \rho U(\rho,z) = \lim_{z \to \infty} U(\rho,z) = 0 \quad (16)$$

Consequently, the function

$$F(\rho,z,Q) = \rho \left[Q + U(\rho,z) \right] \quad (17)$$

plotted against ρ has the characterisitcs of the curves in Figure 1; $F(\rho,z,Q)$ is zero at $\rho = 0$ and is asymptotic to ρQ for large values of ρ. Since Equation (14) is satisfied for arbitrary β by

$$\beta = F(\rho,z,Q), \quad (18)$$

it can be seen from Figure 1 that for any β there are points in the unhatched area for which Equation (14) is satisfied. Hatched areas represent regions in which $|Q| > 1$.

According to a modification of Liouville's theorem (Ref. 7) the density of non-interacting charged-particles along a trajectory in a magnetic field is constant in time. If it is assumed that the particle density is isotropic and constant over the surface of an infinite sphere which contains no particle sources and which is

6

centered about the magnetic field source, the particle density is isotropic and constant and equal to that at infinity at all points in the completely unshielded regions of the magnetic field. (So long as the incident charged-particle intensity is low, interactions between particles can be ignored.)

With regard to Figure 1, all zones of the figure represent completely-unshielded regions of space except the hatched area and possibly Zones A and B which may be at least partially shielded. As an explanatory example, consider the field of a circular loop of conducting wire in the $z = 0$ plane. In such a field, the magnetic induction vector, $\vec{B}(\rho,z)$ at $z = 0$, is everywhere normal to the $z = 0$ plane, and a particle moving in that plane can never leave it. A trajectory is represented in the figure by a straight line $F = \beta$, $z = 0$, and a particle from infinity will move along this line with decreasing ρ toward one of the curves $Q = \pm 1$, touch, and return to infinity. No particle can penetrate the region $0 < \rho < \rho_c$.

In general, however, particle trajectories corresponding to Figure 1 are confined to a ρ-z plane $F = \beta$ (as can be seen by visualizing a z-axis normal to the F-and ρ-axes in the figure). For large z the curves for $Q = \pm 1$ approach their asymptotic values, $F = \pm \rho$, and so there may be a path around the "potential barrier" into Zone A for particles for which $\beta < \beta_c$. Apparently there is no path into Zone B which is, at least in part, a zone of bound orbits. The regions of space corresponding to Zones A and B are partially shielded; particles can reach points in regions of space corresponding to Zones A and B from certain directions (along certain trajectories).

The region of space $\rho'_c < \rho < \rho_c$ is of special interest; it is completely shielded, according to Figure 1, at least for some range

FIGURE 1

Plots of $F(\rho,z,Q)$ Vs ρ for z Constant and $Q = \pm 1$
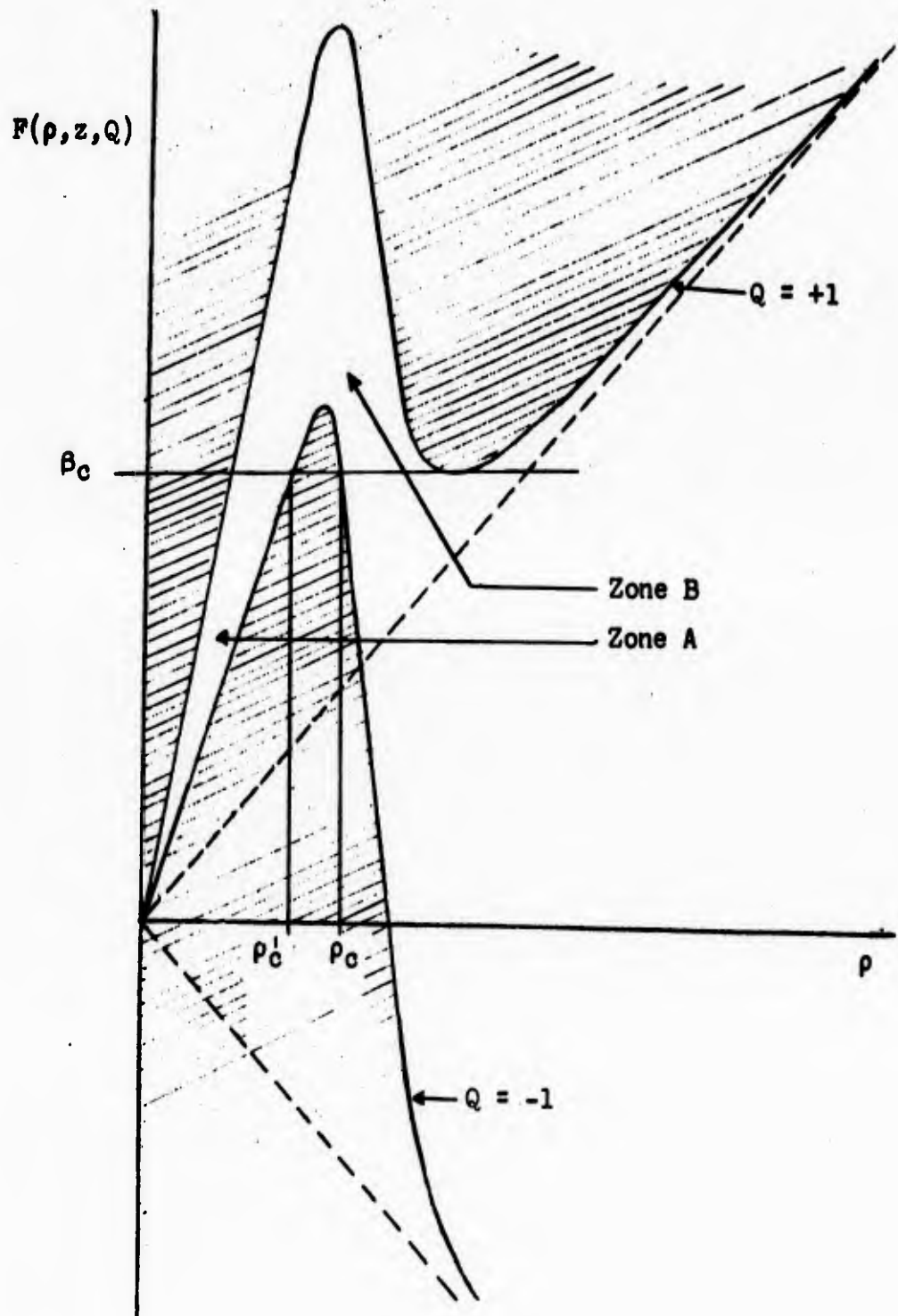
of z. Physically, this region is torcidal in shape and, for a single current loop, is approximately of circular cross section. Upon closer inspection, however, it is observed that the existence of this completely-shielded region depends upon the relative positions of the maximum and minimum values of the curves $F(\rho,z,-1)$ and $F(\rho,z,+1)$. If the maximum of $F(\rho,z,-1)$ is below the minimum of $F(\rho,z,+1)$ this completely-shielded region does not in fact exist. Furthermore, if $U(\rho,z)$ is everywhere less than one, the curve for $F(\rho,z,-1)$ lies below the ρ-axis, $F(\rho,z,+1)$ lies above, and there is no Zone A, probably no Zone B, and no shielding whatsoever.

Levy's analysis of magnetic shielding is based upon a mathematical model involving an infinite current density flowing through a conductor of zero cross-sectional area. His analysis differs in no significant way from the preceding one except his expression for the magnetic vector potential is infinite at the conductor so the functions $F(\rho,z,-1)$ and $F(\rho,z,+1)$ become infinite rather than bounded at a point in $\rho'_c < \rho < \rho_c$. If these functions were indeed infinite at the wire, the existence of the completely shielded region $\rho'_c < \rho < \rho_c$ would be insured. Unfortunately, in reality the magnetic vector potential is everywhere finite and Levy's results may be erroneous.

A more recent investigation of the magnetic shielding provided by a conducting cylinder has been undertaken by Tooper (Ref. 8). Tooper's analysis suffers from the same malady as Levy's: an infinite magnetic potential at the conductor.

The preceding analysis has been quite general. It would appear that practical application of active shielding, at least for configurations under investigation, hinges upon the overlapping of maxima and minima of $F(\rho,z,-1)$ and $F(\rho,z,+1)$ as in Figure 1. If this

9

overlapping does not exist for some practical configuration of solenoids, the utilization of magnetic fields as a shield against charged particles will have suffered a serious setback. The problem requires further study.

2.2 Application to Continued Study

The analysis of the previous section based upon Equations (14) and (15) leads to the conclusion that the feasibility of magnetic shielding has not been adequately examined. The following discussion is pertinent to the problem.

In terms of scaled coordinates ρ and z, shielding is independent of incident particle energy and the existence of completely shielded regions depends only upon the current density $j(\rho',z')$, as is apparent from Equation (15). This is, the existence of completely shielded regions depends only upon the relative positions of conducting circuit elements and direction and magnitude of the respective currents. For shielding against incident charged particles of given energy, the effectiveness of a given physical configuration is a function of the scale factor C, Equation (13), and hence depends upon the size of the configuration. Practical considerations will fix the necessary shielding energies and the configuration size, and hence will fix C in terms of the current density factor j_s. Shielding will depend upon the relative magnitudes of currents in the various circuit elements (obviously).

Taking all aspects of the preceding discussion into consideration, it is reasonable to believe that a configuration can be found which will shield a given volume against charged particles of energies less than a given cut-off energy, provided high enough currents

10

are obtainable. But the requirements of superconductivity place an upper limit upon the current density in any given circuit. Indeed, it is doubtful if present superconductor technology is adequate and reasonable extrapolations based upon possible expectations of future progress may be necessary. Although some insight has been gained with regard to the interrelation of the various parameters of the problem, analysis is far from complete. Any conclusion as to the utility of magnetic shielding based upon proposed configurations requires further study.

The Appendix contains a series evaluation of the integral for the magnetic vector potential $\vec{A}$ for a rectangular cross-section solenoid. The resultant equations can be used to study the magnetic shielding of a single solenoid, or since magnetic fields are additive, they may be used to study the shielding resulting from any number of solenoids centered about a common axis. Thus, for N such solenoids,

$$U(\rho,z) = \sum_{n=1}^{N} \frac{J_n}{J_s} U_n(\rho,z) \tag{18}$$

where J_n is the current density in the nth solenoid and the nth term of the series represents the magnetic vector potential of that solenoid. It is noted that the $U_n(\rho,z)$ are non-negative and the contribution of the nth solenoid to $U(\rho,z)$ depends upon its size and location and upon the magnitude and sign of J_n. An axially symmetric field can be adequately approximated by utilizing a sufficiently large number of solenoids possessing appropriate cross-sectional area and current density.

11

The Appendix also contains equations for the magnetic field $\vec{B}$.
It will be necessary to utilize these equations to determine the upper bound for possible values of current density j.

3. EXPERIMENTAL INVESTIGATION

The objective of the experimental investigation was to establish the capability of winding superconducting solenoids and of making junctions between the superconducting wire and current carrying leads. These problems present formidable obstacles to the design and construction of superconducting active radiation shields. An account of the experimental investigation follows.

3.1 Junction Development

Twenty different junctions between niobium-zirconium superconductors and normal conductors were assembled and tested at liquid helium temperatures to determine junction resistance and maximum current capacity. The wire, Supercon B-33 obtained from Supercon of Houston, was 67% niobium and 33% zirconium by atomic ratio, and was .010 inches in diameter. Its characteristics is short samples are guaranteed to be within 10% of the values shown in Figure 2. Because the wire will not wet with low temperature solder and because brazing results in temperatures high enough to anneal the wire, ultrasonic soldering, plating, crimping, clamping, and spot welding were attempted using various surface cleansers. Most of these junctions have been described in the literature, but no reference to spot welding copper foil to superconducting wire was found. The junction preparation and results are shown in Table I. The most promising of these junctions were built and tested repeatedly to determine reliability. Spot welding produced consistently superior results in reliability, simplicity, and high current capacity.

13

FIGURE 2 - CRITICAL CURRENT OF Nb-33% Zr AS A FUNCTION OF TRANSVERSE MAGNETIC FIELD
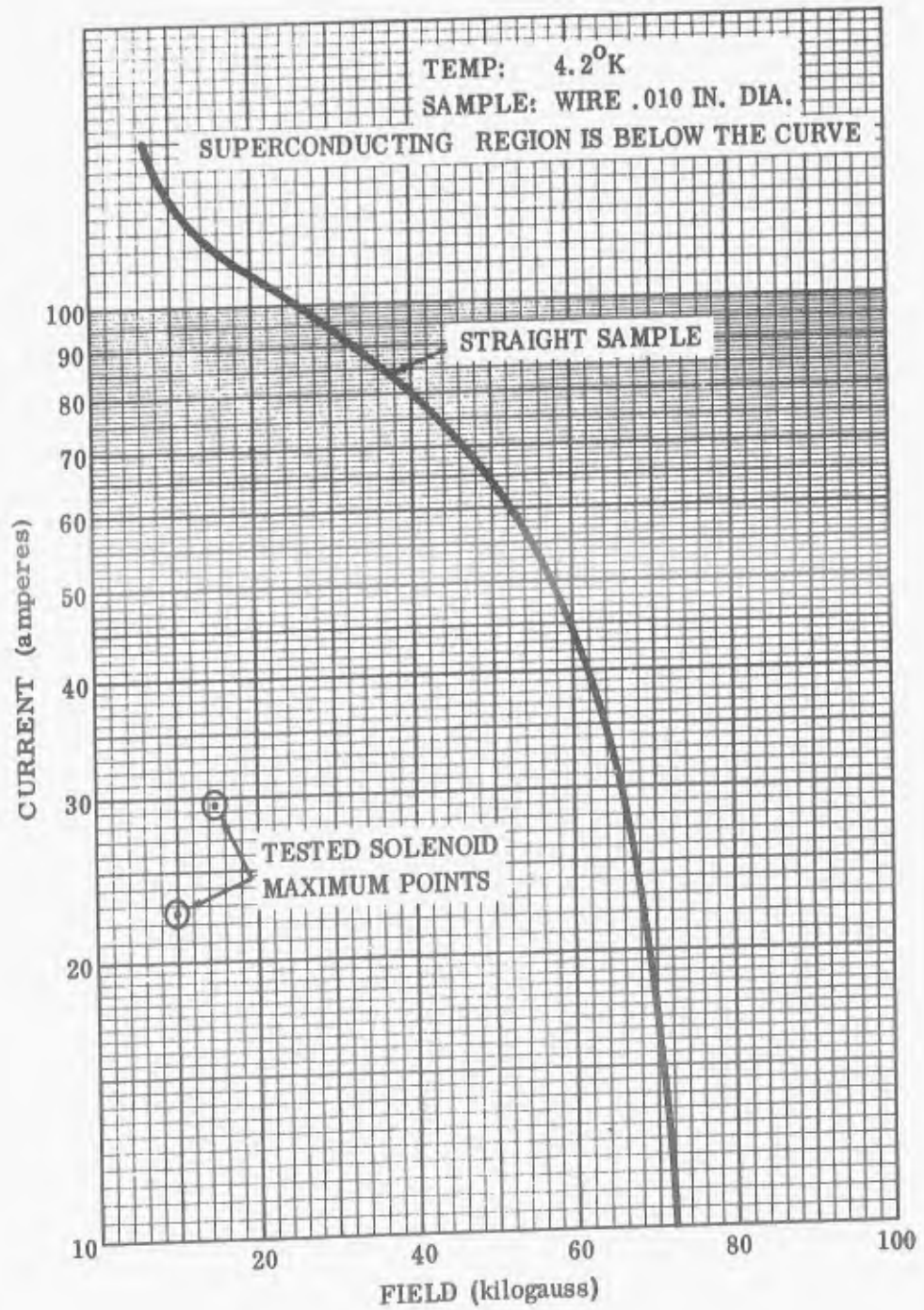

TEMP: 4.2°K
SAMPLE: WIRE .010 IN. DIA.
SUPERCONDUCTING REGION IS BELOW THE CURVE

STRAIGHT SAMPLE

TESTED SOLENOID
MAXIMUM POINTS

CURRENT (amperes)

FIELD (kilogauss)

Table I

Exploratory Junctions

Lead to be Joined	Method of Cleaning	Method of Connecting	Resistance (micro-ohms)	Maximum Current (amps)
1/8" diam. copper tube	None	Tube crushed (around Nb-Zr)	Low	9.0
1/8" diam. copper tube	Wire in NaCN	Tube crushed	170	Low
1/8" diam. copper tube	Wire in NaCN	Tube crushed	78	Low
1/8" diam. copper tube	Wire in NaCN, H_2SO_4	Tube crushed	0.7	21
1/8" diam. copper tube	Wire in NaCN, H_2SO_4	Tube crushed	400	Low
1/8" diam. copper tube	Tube in hot alkaline solution	Copper plated Nb-Zr, PbSn tinned, tube crushed	Low	3.0
1/8" diam. copper tube	same as above, but indium tinned	Indium tinned Nb-Zr tube crushed	High	Low
1/8" diam. copper tube	Tube in H_2SO_4		10	Low
.005-in. copper foil	None	12 spot welds	.25	75
12 ga. copper wire	None	Fused with torch	2.0	20
12 ga. copper wire	None	Fused with torch	500	Low
Nb-Zr wire	None	Fused with torch	High	Low
Nb-Zr wire	None	one spot weld	0.1	82
Nb-Zr wire	None	One spot weld	0.4	76
Nb-Zr wire	Emery paper	Flattened Nb-Zr clamped together	14	Low
.02-in. Pb foil	H_2SO_4	Foil crushed around Nb-Zr	High	Low

15

Table I (Cont'd)

Lead to be Joined	Method of Cleaning	Method of Connecting	Resistance (micro-ohms)	Maximum Current (amps)
.02-in. Pb foil	H_2SO_4	Foil crushed around Nb-Zr	High	Low
Indium tinned copper blocks	Wire-emery paper	Nb-Zr clamped between blocks	24	Low
Indium tinned copper blocks	Wire-emery paper	Nb-Zr clamped between blocks	24	Low
12 ga. copper wire	Degrease	Conductive epoxy	High	Low
12 ga. copper wire	Degrease	Conductive lacquer	High	Low
12 ga. copper wire	Degrease	Conductive enamel	High	Low
12 ga. copper wire	None	Nb-Zr copper plated PbSn soldered	300	Low
12 ga. copper wire	None	8" Nb-Zr copper plated PbSn soldered	14	2.4
.0015-in. copper foil	None	12 spot welds	Low	12
12 ga. copper wire	Ultrasonic	Ultrasonic indium soldered	250	Low

Several attempts were made to copper and gold plate wire using different baths and alkaline and acid cleaners. These wires were rejected because the plating flaked off when the wire was flexed.

For the sake of uniformity, all but one sample were tested using 1-in. of wire for the junction.

16

Since copper has a higher heat and electrical conductivity than Nb-Zr, satisfactory welds with little wire deformation were obtained only after many trials. A Hughes spot welder was used. While welding superconducting wires to copper foil, the welding electrodes pressed the wire and foil together with a force of 3 pounds,and 35 to 45 watt-seconds of energy were used. A copper electrode 2 mm wide pressed the wire to a 0.005 inch thick copper foil held in place by a domed steel electrode with a 1.5 mm radius. Wires were joined by the use of flat copper electrodes 2 mm wide, with 3 pounds of force, and 5 to 6 watt-seconds of energy. The high temperature transient caused by spot welding did not seriously deteriorate the wire's ability to carry high currents in a magnetic field. Critical currents in excess of 70.0 amperes were measured with the junctions in a 10.0 kilogauss field and with $\ddot{H}$ perpendicular to the wire. The copper foil to which the Nb-Zr wires were spot welded was easily soft soldered to copper current leads. An assembly of twelve junctions is shown at the left in Figure 3.

3.2 Solenoid Winding and Testing

Three superconducting solenoids were wound and four were tested. These solenoids are shown in Figure 3. The fourth solenoid (at the center of the figure) was obtained from Dr. B. C. Deaton of General Dynamics/Fort Worth and was constructed of niobium 25% zirconium wire manufactured by Wah Chang Corporation. The solenoid was wound in GD/FW motor winding shop under the direction of Dr. Deaton. Each turn was insulated from adjacent turns by a .010 inch diameter nylon thread and each layer was insulated with .0015 inch copper foil. The finished solenoid contained 4000 feet of .010 inch diameter

17

FIGURE 3 – EXPERIMENTAL JUNCTIONS AND SOLENOIDS
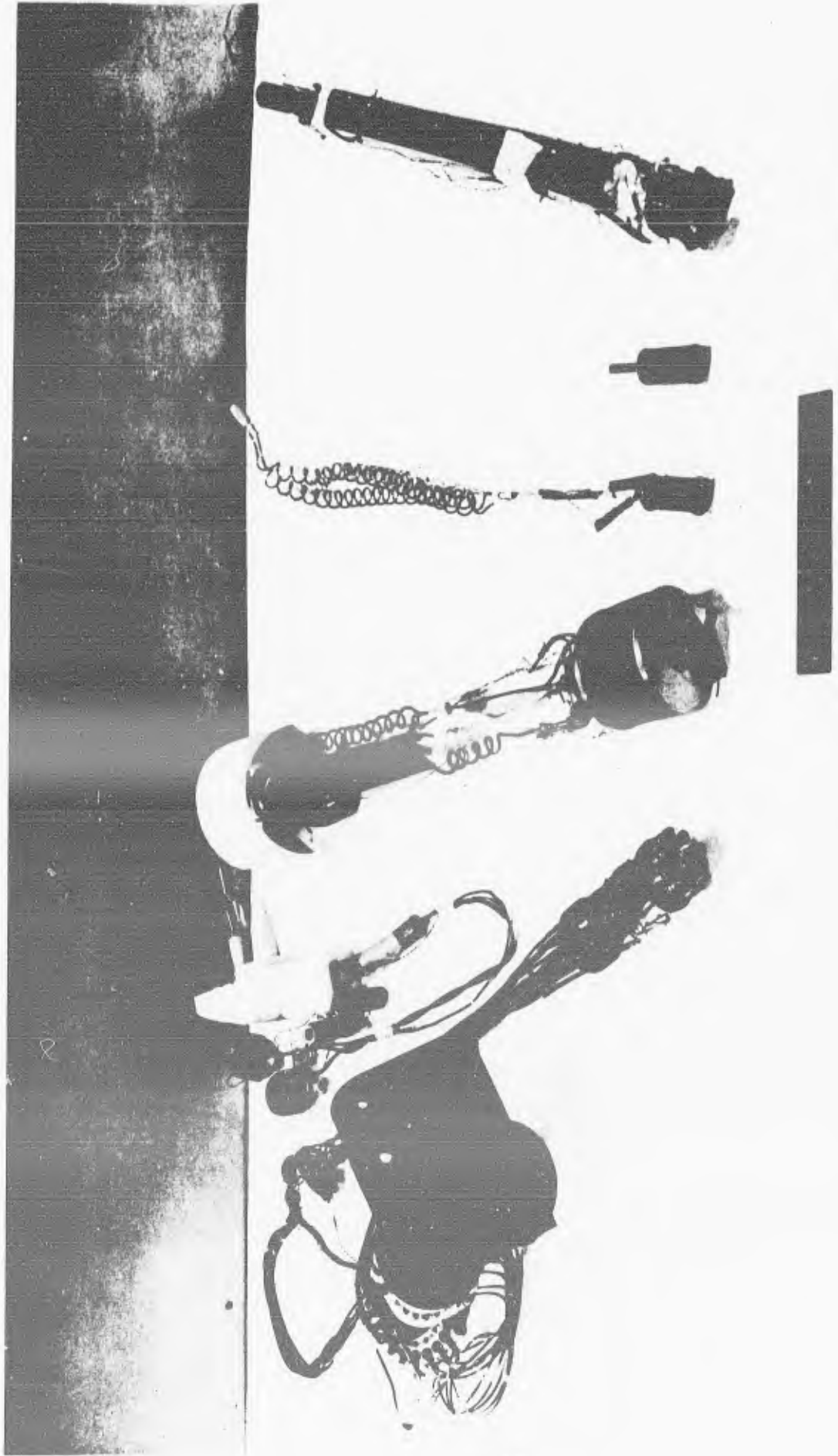
wire in 7600 turns and had an inside diameter of 1.125 inches. This solenoid did not perform well with its crimped copper current leads. After spot welded leads were attached the performance improved many-fold. The maximum operating point for this solenoid is shown in Figure 4, along with typical results found in the literature for this alloy wire (Refs. 9, 10, and 11). The copper foil between layers was a good insulator because: 1) in comparison to the zero resistance of superconducting wire it had a high resistance; 2) it helped carry heat out of the solenoid on cool down; and 3) when the solenoid reached its maximum operating point and the superconductor returned to normal resistance, the copper slowed the field collapse and reduced heating and arcing of the windings by carrying most of the induced current. However, it was also a poor insulator because it slowed field buildup by shorting the windings when self-inductance produced more than 25 millivolts across the solenoid.

The other three solenoids were wound using Supercon B-33 Nb-Zr. Two of these had insulation between layers and no insulation between turns. The other had no insulation at all and was built to see how effective surface oxides and drawing lubricant were as insulation. Since this solenoid produced no magnetic field poor insulation was indicated. The other two solenoids departed from solenoidal current flow only when the current was increased too rapidly. Differences in construction may explain the absence of complete insulation breakdown in these two solenoids as opposed to the one with no insulation. The operating solenoids 1) were insulated layer from layer by .0015 inch thick copper foil, 2) had only minor pressure between adjacent turns, and 3) had each layer saturated with a

19

FIGURE 4 - CRITICAL CURRENT OF Nb-25% Zr AS A FUNCTION
OF TRANSVERSE MAGNETIC FIELD
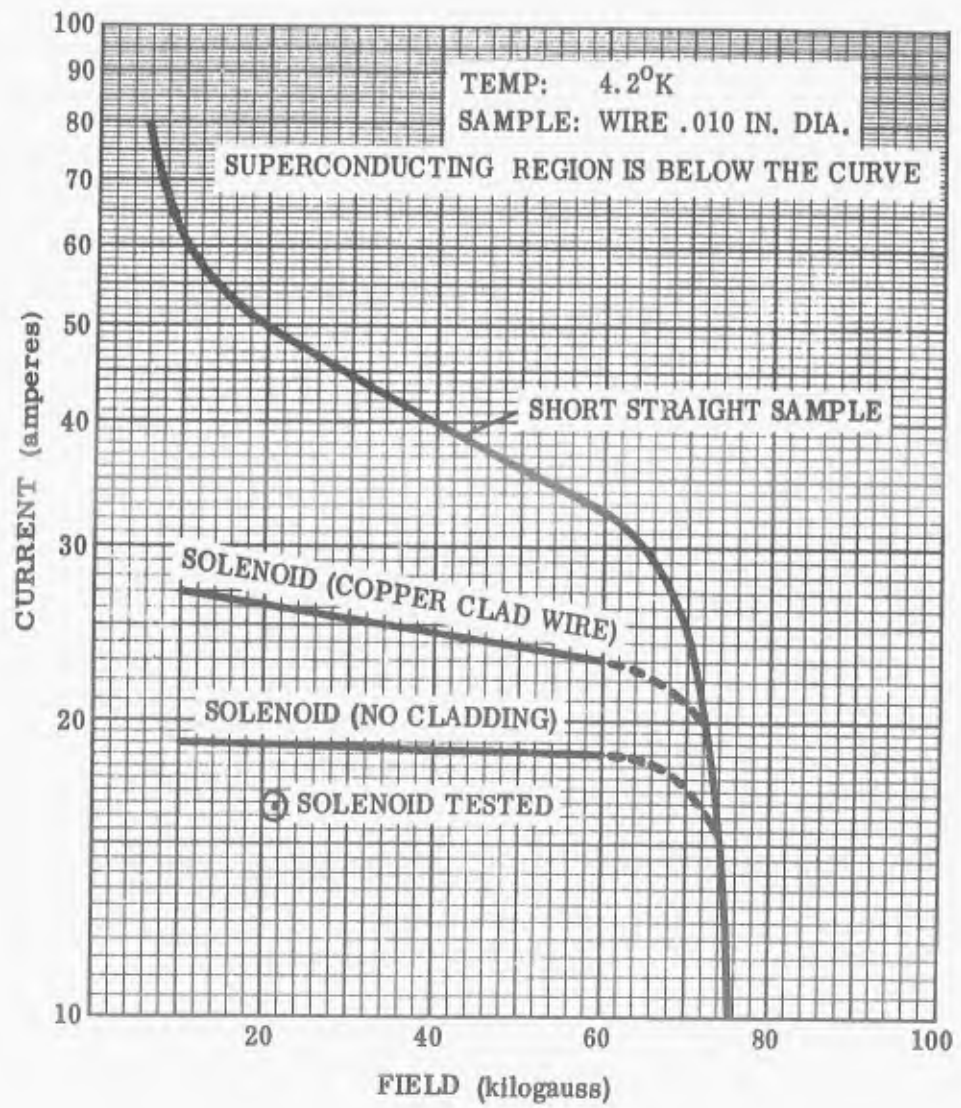
sprayed-on insulator, "Krylon." The non-operating solenoid had
1) intimate contact between layers due to a wire tension of 2
pounds applied during winding, 2) no layer insulation, and 3)
no sprayed-on insulator.

The first of the two operating solenoids contained 500 feet
of .010-inch diameter, 33% Zr wire in 1650 turns and had an inside
diameter of .868 inches. Its maximum operating point is the lower
of the two points in Figure 2. The second solenoid contained 480
feet of .01-inch diameter, 33% Zr wire in 3550 turns and had an
inside diameter of 0.26 inches. Its maximum superconducting point
is the higher of the two points. None of the solenoids suffered
deterioration upon exceeding the critical current.

3.3 Critical Current Depression in Solenoids

The depression of current-carrying capacity of superconducting
wire when in solenoidal form was attributed to non-uniform wire by
early workers. However, a 1000-foot length of wire, wound induc-
tively carried only a fraction of the short sample current, but when
the wire was wound non-inductively its behavior was very close to
that of a short sample. Although a slight separation of the super-
conducting wires is reported to improve performance (Refs. 9 and 12),
results pertaining to the solenoid tested shown in Figure 4 do not
substantiate this claim. The turns of this solenoid were separated
by .01 inches and the layers, by .0015 inches. J. K. Hulm (Ref. 9)
tentatively suggests a "flux-jump" model to explain current depres-
sion. Cryophysicists agree superconduction in Nb-Zr is isolated in
many filaments throughout the alloy (these appear to be along strain
or defect lines). Magnetic flux, according to the flux-jump model,

21

does not penetrate the wire smoothly but must proceed stepwise from filament (or group of filaments) to filament. Each time it crosses a filament, superconductivity is destroyed temporarily and some local heating is produced. This model is in agreement with the observation that a solenoid seldom goes normal in the region of highest field but it does not explain some of the characteristics of short samples.

One group reported achievement of identical solenoid and short sample behavior. J. O. Betterton and G. D. Kneip (Ref. 11) report a solenoid and short sample current limit of 40 amperes at 22 kilogauss in 10-mil wire that they fabricated. Two contributing influences to this encouraging result were named: inconel cladding of the wire and special heat-treat and drawing procedures. (G. D. Kneip has since joined Supercon and was instrumental in the production of the wire used in this research report.) Subsequent literature (Refs. 9 and 13) indicate that these favorable results have not been reproducible. D. B. Montgomery (Ref. 12) argues convincingly that the depression problem in solenoids is due to induced persistent currents in the superconductor that oppose field build-up. These are the same currents that produce apparent diamagnetism in superconducting magnets. The sum of induced currents and applied currents equals the critical current of a straight sample. The induced current is estimated from a measurement of the residual field after the applied current is reduced to zero. These persistent currents are locally destroyed when a section of the coil goes normal. This mechanism is compatible with the phenomena that gave rise to the flux-jump model. When viewed in the light of the results reported in Reference 13, the

22

does not penetrate the wire smoothly but must proceed stepwise from filament (or group of filaments) to filament. Each time it crosses a filament, superconductivity is destroyed temporarily and some local heating is produced. This model is in agreement with the observation that a solenoid seldom goes normal in the region of highest field but it does not explain some of the characteristics of short samples.

One group reported achievement of identical solenoid and short sample behavior. J. O. Betterton and G. D. Kneip (Ref. 11) report a solenoid and short sample current limit of 40 amperes at 22 kilogauss in 10-mil wire that they fabricated. Two contributing influences to this encouraging result were named: inconel cladding of the wire and special heat-treat and drawing procedures. (G. D. Kneip has since joined Supercon and was instrumental in the production of che wire used in this research report.) Subsequent literature (Refs. 9 and 13) indicate that these favorable results have not been reproducible. D. B. Montgomery (Ref. 12) argues convincingly that the depression problem in solenoids is due to induced persistent currents in the superconductor that oppose field build-up. These are the same currents that produce apparent diamagnetism in superconducting magnets. The sum of induced currents and applied currents equals the critical current of a straight sample. The induced current is estimated from a measurement of the residual field after the applied current is reduced to zero. These persistent currents are locally destroyed when a section of the coil goes normal. This mechanism is compatible with the phenomena that gave rise to the flux-jump model. When viewed in the light of the results reported in Reference 13, the

22

induced current mechanism is also compatible with the first appearance of normal resistance in low-field portions of a solenoid.

In the present study, the field strength per ampere was calculated for each solenoid according to the Fabry formulation (Ref. 14). The magnetic fields of the solenoids were from 83% to 50% of the predicted values. Field measurements were made in two independent ways one with a Grassot-type fluxmeter (Ref. 15), and the other using the magneto-resistance of copper (Ref. 16). The fluxmeter was checked against an accurately calibrated magnet normally used in nuclear magnetic resonance equipment. An attempt to build a magneto-resistance probe made of indium based on the work of P. Cotti (Ref. 17) produced negative results.

3.4 Persistent Current Electromagnets

Two of the solenoids were operated in the closed loop or persistent current mode. This mode was easily accomplished by providing a superconducting current path outside the solenoid that could be switched off or on. A short piece of Nb-Zr wire was wound around a carbon resistor and thermally insulated so that the wire could be heated and made non-superconducting while in a liquid helium bath. The ends of this superconducting switch were spot welded to the current leads of the solenoid. Startup was accomplished by heating the switch so that current passed through the solenoid. When the desired field was reached, the heated section was allowed to cool and the power supply was turned off leaving a persistent current flowing through the solenoid and the superconducting switch. Existence of this current was indicated by a steady magnetic field.

23

To make the switch, approximately fifteen turns of wire were wrapped around a 0.1-watt, 22,000-ohm carbon resistor and the two were thermally insulated from helium by wrapping with four layers of masking tape. Fifty-seven volts across the resistor would switch off the circuit within one second. Switch-on time was less than five seconds. Power dissipated by the resistor was only 32 milliwatts (its resistance increased to 100,000 ohms when operated near liquid helium temperature).

3.5 Cryogenic System

The solenoids were tested in liquid helium in a 3-liter capacity strip-silvered-glass dewar. This dewar was nested in a liquid nitrogen dewar. The combination is shown in Figure 5. Current carrying leads were two 10- or 12-gauge Formvar insulated copper wires which were thermally insulated with styrofoam from below the top of the helium dewar to 2 inches below the top of the second dewar. In the second dewar the wires were immersed in a liquid nitrogen bath and then were connected to a current source. The liquid nitrogen provided a temperature buffer between liquid helium and ambient temperature. Four to five inches below the top of the helium dewar the copper wires terminated and the current was carried to the superconductor by two .005 inch thick copper foils. The large surface areas of the foils were used to take advantage of helium vapor cooling. This system resulted in liquid helium consumption of from 100 cc to 200 cc per hour depending on the current in the copper leads.

3.6 Instrumentation and Equipment

Development equipment and instrumentation are shown in Figure 5. From left to right are a Drussen and Barnes Corporation constant-

24

FIGURE 5 – CRYOGENIC EQUIPMENT

25
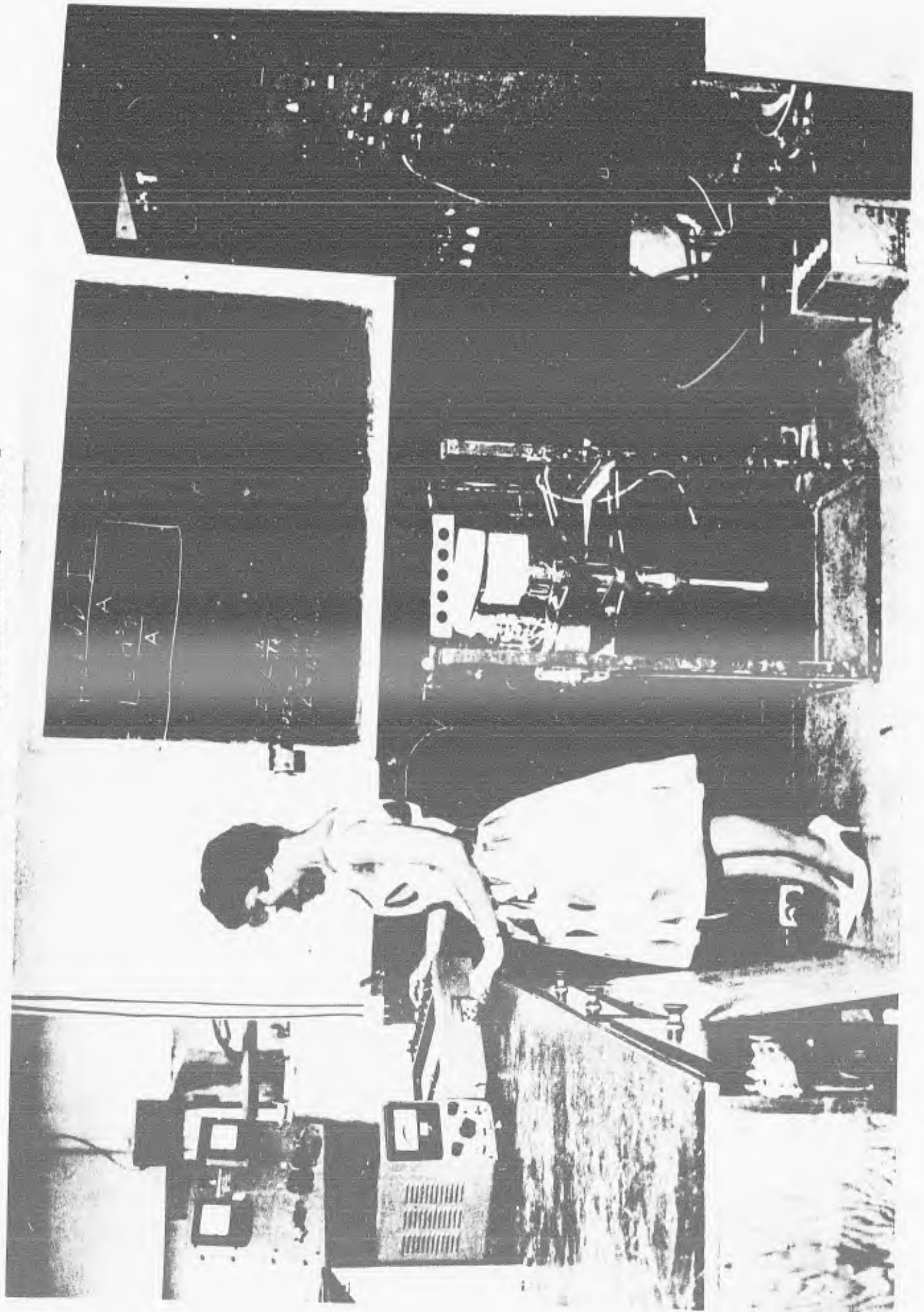
current supply, a Hewlett-Packard microvolt meter, a Moseley X-Y recorder, a liquid nitrogen dewar, a liquid helium dewar, a 150-ampere capacity transistorized current controller and ammeters in the tall rack, and batteries, charger, and protective relay in the short rack.

The constant current supply held the current through the magneto-resistance probe steady, while the voltage across the probe was indicated on the microvoltmeter and on the Y-axis of the Moseley recorder. The X-axis indicated current through the solenoid. The microvoltmeter was also used to measure junction resistance. Voltage across the junction was displayed on the meter and plotted on the recorder Y-axis while the current through the junction was plotted on the X-axis.

4. CONCLUSIONS AND RECOMMENDATIONS

4.1 Theoretical Study

Critical examination of available literature leads to the conclusion that the feasibility of magnetic shielding has not been adequately established. Systematic studies should be undertaken to determine optimum shielding geometries for the protection of space vehicles of given size and shape. An optimum shielding geometry should provide a given volume with a predetermined amount of protection by use of a minimum of superconducting circuitry. Practical considerations of present superconductor technology (and future expectations if necessary) should be considered. Weight studies of promising optimum shielding geometries should be made for comparison with equivalent passive shielding. The study should proceed along the following lines:

1. Consideration should be given to the determination of likely space-vehicle shielding requirements. It appears that shielding for spheres, cylinders, and toroids of various sizes should be studied. Indeed, requirements of active shielding may determine space vehicle shapes.

2. The shielding provided by various configurations of superconducting rings should be determined for given space vehicle shapes and sizes. The equations derived in section 2.1 and in the Appendix should be used. Because of the complexity of the expressions for the magnetic vector potential, an IBM 7090 code will be necessary. Optimum shielding geometries should be sought in preliminary investigations without regard to weight and superconductivity requirements.

27

3.   Upon conclusion of preliminary investigations, practical considerations of the requirements of superconductivity should be applied to preliminary optimum shielding geometries. Revisions in shielding configurations will probably be necessary to insure feasibility.

4.   The weights of optimum configurations should be computed upon completion of step 3 by taking into account the weights of necessary structural support and of superconducting elements. Preliminary calculations need not include the weight of cryogenic equipment, etc.

5.   Upon completion of step 4, it will undoubtedly be necessary to iterate steps 2, 3, and 4 to improve any given configuration. Improvements and modifications of the optimization method involving more detail in superconductor requirements and weight calculations should be made. Ultimately a digital computer code may be devised using the methods of linear programming to handle the whole problem.

4.2 Experimental Investigations

Spot welded connections between leads and superconducting wire were quite satisfactory because they could be made with ease and because critical currents higher than 70 amperes are unlikely in solenoids of the wire size utilized. However, since spot welds produced a high current interface between superconductor and copper in a small area, a well-bonded coat of electroplated copper should produce a superior junction. It is thought a well-bonded plate was not produced during this development program. Procedures for electroplating were those recommended in References 18 and 19 and also in a private communication with H. F. Scott of RCA. All electrodeposits

28

that were made flaked off to some extent at points where the Nb-Zr wire was pushed beyond its elastic limit.

The apparent reduction in critical current of superconducting wire wound in solenoids is possibly due to induced currents that oppose field change. This uncertainty in performance characteristics requires extreme conservatism in the design of a magnet to produce a given field.

It may be possible to obtain short-sample critical-currents in superconducting magnets by one or both of the following approaches:

1. Wind the wire in a toroid in a force-free geometry as in Reference 13.

2. Wind the wire in the form of an assembly of parallel loops so that the field is built up in a series of induced current increases (Ref. 20).

Protection of small solenoids from heating due to field collapse was accomplished. However, larger systems will require more complex devices, such as several tentatively suggested in Reference 21. The adequacy of these devices has not been tested.

It might be added that, to date, only comparatively small superconducting coils have been investigated whereas active shielding configurations will probably require windings of some tens of feet in radius. Such large solenoids must be investigated if active shielding is to be utilized.

APPENDIX

THE MAGNETIC VECTOR POTENTIAL AND
FIELD OF A RECTANGULAR CROSS SECTION SOLENOID

Equations for the magnetic vector potential $\vec{A}$ and the field $\vec{B}$ are to be derived for a rectangular cross section solenoid as shown in Figure 6. Since $\vec{A}$ has rotational symmetry about the Z-axis, the field point $\vec{r}$ can be taken in the X-Z plane. Cylindrical coordinates are used, as shown in Figure 7. In the MKS system, the expression for the magnetic vector potential is

$$\vec{A}(\vec{r}) = \frac{\mu_0}{4\pi} \int_{Vol.} \frac{\vec{j}(\vec{r}')}{|\vec{r} - \vec{r}'|} \, d^3\vec{r}' \tag{1}$$

and for the chosen geometry this reduces to

$$\vec{A} = 1_y A \tag{2}$$

where

$$A = \frac{\mu_0 j}{4\pi} \int_a^b \int_0^{2\pi} \int_h^k \frac{\rho\cos\emptyset}{\sqrt{x^2 - 2x\rho\cos\emptyset + \rho^2 + (z-z')^2}} \, dz' \, d\emptyset \, d\rho \tag{3}$$

It is assumed that $j(\rho, z')$ is constant throughout the conductor. Integration over z' yields

$$A = \frac{\mu_0 j}{4\pi} \int_a^b \int_0^{2\pi} \rho\cos\emptyset \left[\sinh^{-1}\frac{k-z}{\sqrt{x^2 - 2x\rho\cos\emptyset + \rho^2}} \right.$$

$$\left. -\sinh^{-1}\frac{h-z}{\sqrt{x^2 - 2x\rho\cos\emptyset + \rho^2}} \right] d\emptyset \, d\rho \tag{4}$$

FIGURE 6   RECTANGULAR CROSS SECTION SOLENOID
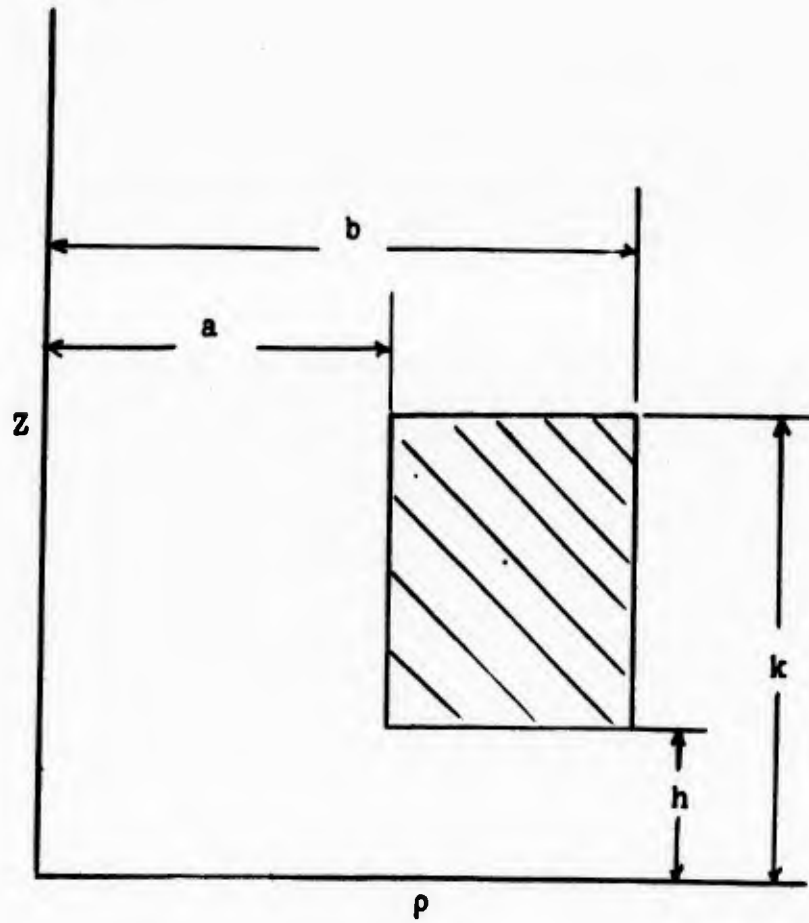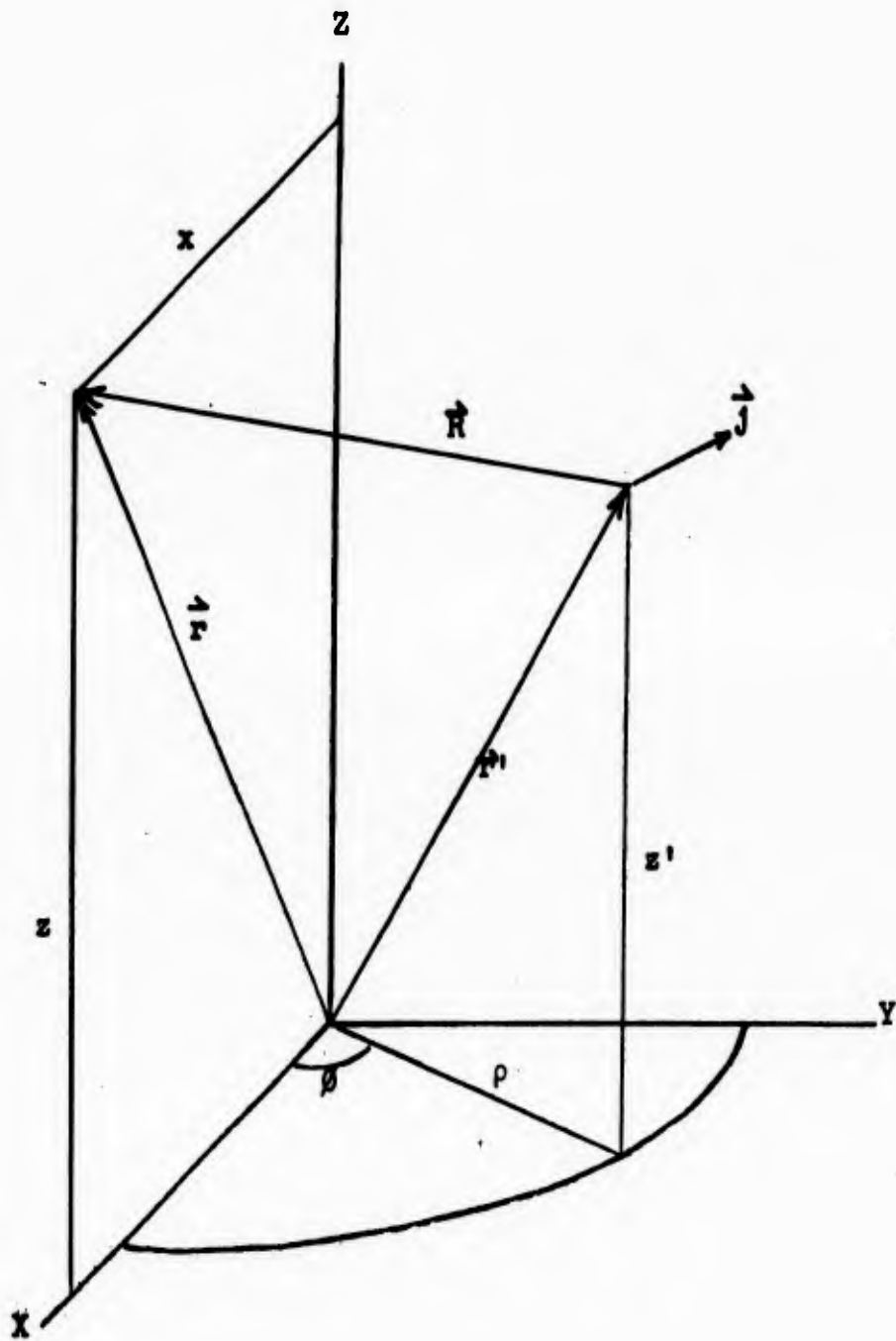a and b are inner and outer radii respectively;
k-h is the length

FIGURE 7   SYSTEM OF COORDINATES

Set

$$Q(x,u) = \int_a^b \int_0^{2\pi} \rho\cos\phi \sinh^{-1}\frac{u}{\sqrt{x^2-2x\rho\cos\phi+\rho^2}} \, d\phi d\rho \qquad (5)$$

so

$$A(x,z) = \frac{\mu_0 j}{4\pi} \left[Q(x,k-z) - Q(x,h-z) \right] \qquad (6)$$

Since

$$Q(x,u) = - Q(x,-u) \qquad (7)$$

u can be considered non-negative. Let

$$I(x,\rho;u) = \int_0^{2\pi} \cos\phi \sinh^{-1}\frac{u}{\sqrt{x^2-2x\rho\cos\phi+\rho^2}} \, d\phi \qquad (8)$$

so

$$Q(x,u) = \int_a^b \rho \, I(x,\rho;u) d\rho \qquad (9)$$

The Maclaurin's series expansion for $\sinh^{-1} z$ is

$$\sinh^{-1} z = \sum_{n=0}^{\infty} (-)^n \frac{\Gamma(n+1/2)}{\Gamma(1/2)n!} \frac{z^{2n+1}}{2n+1}, \quad |z|<1 \qquad (10)$$

With

$$z = \frac{u}{\sqrt{x^2-2x\rho\cos\phi+\rho^2}} \leq \frac{u}{|x - \rho|} < 1, \; x \neq \rho, \qquad (11)$$

Equation (8) becomes

$$I(x,\rho;u) = \sum_{n=0}^{\infty} (-)^n \frac{\Gamma(n+1/2)}{\Gamma(1/2)n!} \frac{u^{2n+1}}{2n+1} \int_0^{2\pi} \frac{\cos\phi}{(x^2-2x\rho\cos\phi+\rho^2)^{n+1/2}} \, d\phi \qquad (12)$$

33

for $u < |x-\rho| \neq 0$. The interchange of summation and integration is justified at least for $u < |x-\rho| \neq 0$ since the series is uniformly convergent on this range. Now

$$x^2 - 2x\rho\cos\phi + \rho^2 = x^2(1 - \frac{\rho}{x} e^{i\phi})(1 - \frac{\rho}{x} e^{-i\phi}) \tag{13}$$

and so by the binominal series

$$\frac{1}{(x^2 - 2x\rho\cos\phi + \rho^2)^{n+1/2}}$$

$$= \frac{1}{x^{2n+1}} \sum_{k=0}^{\infty} \frac{\Gamma(n+k+1/2)}{k!\Gamma(n+1/2)} \left|\frac{\rho}{x}\right|^k e^{ik\phi} \sum_{m=0}^{\infty} \frac{\Gamma(n+m+1/2)}{m!\Gamma(n+1/2)} \left|\frac{\rho}{x}\right|^m e^{-im\phi}. \tag{14}$$

The two series are absolutely convergent for $\rho < x$, and it is known that the series representing the product of two absolutely convergent series is absolutely convergent and can be summed in any order. Furthermore,

$$\int_0^{2\pi} \cos\phi \, e^{ik\phi} \, d\phi = 0 \tag{15}$$

for $|k|$ equal to 0 or any integer except 1, so for $\rho < x$,

$$\int_0^{2\pi} \frac{\cos\phi}{(x^2 - 2x\rho\cos\phi + \rho^2)^{n+1/2}} \, d\phi$$

$$= \frac{2\pi}{\left[\Gamma(n+1/2)\right]^2 x^{2n+1}} \sum_{m=0}^{\infty} \frac{\Gamma(n+m+1/2)\,\Gamma(n+m+3/2)}{m!\,(m+1)!} \left|\frac{\rho}{x}\right|^{2m+1}. \tag{16}$$

This expression becomes valid for $\rho > x$ if ρ and x are interchanged.

34

The combination of Equations (12) and (16) yields

$$I(x,\rho;u) = \sqrt{\pi} \sum_{n=0}^{\infty} \frac{(-)^n}{n!\,\Gamma(n+3/2)} \left(\frac{u}{x}\right)^{2n+1} \sum_{m=0}^{\infty} \frac{\Gamma(n+m+1/2)\Gamma(n+m+3/2)}{m!\,(m+1)!} \left(\frac{\rho}{x}\right)^{2m+1}$$

$$= \sqrt{\pi} \sum_{m=0}^{\infty} \frac{1}{m!\,(m+1)!} \left(\frac{\rho}{x}\right)^{2m+1} \sum_{n=0}^{\infty} (-)^n \frac{\Gamma(n+m+1/2)\Gamma(n+m+3/2)}{n!\,\Gamma(n+3/2)} \left(\frac{u}{x}\right)^{2n+1}$$

$$= 2 \sum_{m=0}^{\infty} \frac{\Gamma(m+1/2)\Gamma(m+3/2)}{m!\,(m+1)!} \left(\frac{\rho}{x}\right)^{2m+1} \frac{u}{x} F\left\{m+1/2, m+3/2; 3/2; -\left(\frac{u}{x}\right)^2\right\}, \quad (17)$$

at least for $u \le |x - \rho|$, $\rho < x$, where F is the hypergeometric function. The interchange of summations is justified since Equation (16) is uniformly convergent for $\rho < x$ and Equation (12) is uniformly convergent for $u < |x-\rho| \ne 0$. The latter is true because

$$\int_0^{2\pi} \frac{\cos\phi}{(x^2 - 2x\rho\cos\phi + \rho^2)^{n+1/2}} \, d\phi \le \frac{2\pi}{|x-\rho|^{2n+1}}, \quad x \ne \rho \qquad (18)$$

Equation (17) is valid for $\rho > x$, $u < |\rho-x|$, when ρ and x are interchanged.

The hypergeometric function can be expressed as an integral as follows

$$F(a,b;c;-z) = \frac{1}{2\pi i} \frac{\Gamma(c)}{\Gamma(a)\Gamma(b)} \int_{-i\infty}^{i\infty} \frac{\Gamma(a+s)\Gamma(b+s)\Gamma(-s)}{\Gamma(c+s)} z^s \, ds \qquad (19)$$

where $|\arg z| < \pi$ and

$$\max\left\{R(-a), R(-b)\right\} < R(s) < 0 \qquad (20)$$

35

(Ref. 22, page 62). By making use of the asymptotic expansion for gamma functions

$$\ln\Gamma(a+z) = (a+z-1/2)\ln z - z + \ln\sqrt{2\pi} + 0(1/z) \tag{21}$$

for $\left|\arg z\right| < \pi$ (Ref. 22, page 48) and the expression

$$\Gamma(z)\,\Gamma(1-z) = \frac{\pi}{\sin\pi z} \tag{22}$$

(Ref. 22, page 3) it can be shown that as $|t|$ approaches infinity

$$\frac{\Gamma(a+s)\Gamma(b+s)\Gamma(-s)}{\Gamma(c+s)} = 0\left\{e^{-\pi|t|}\,s^{a+b-c-1}\right\} \tag{23}$$

where $s = \beta + it$. Then, since the integrand is finite, there is a constant A such that

$$\left|\frac{\Gamma(a+s)\Gamma(b+s)\Gamma(-s)}{\Gamma(c+s)}\right| < A\,e^{-\pi|t|}(\beta^2 + t^2)^{\frac{a+b-c-1}{2}} \tag{24}$$

for all t, and hence

$$\left|\frac{1}{2\pi i}\int_{-i\infty}^{i\infty}\frac{\Gamma(a+s)\Gamma(b+s)\Gamma(-s)}{\Gamma(c+s)}\,z^s\,ds\right| \tag{25}$$

$$\leq \int_{-\infty}^{\infty}\frac{A}{2\pi}\,z^\beta\,e^{-\pi|t|}\,(\beta^2+t^2)^{\frac{a+b-c-1}{2}}\,dt \leq A'\int_0^{\infty}e^{-\pi t}\,(\beta^2+t^2)^{\frac{a+b-c-1}{2}}\,dt$$

for z   real and positive. The parameter β can be any number near zero satisfying Equation (20), so Equation (25) is valid in the limit as β approaches zero since the integral on the right is uniformly convergent. But

$$\int_0^{\infty}e^{-\pi t}\,t^{a+b-c-1}\,dt = \frac{\Gamma(a+b-c)}{\pi^{a+b-c}} \tag{26}$$

36

so, according to Equations (19), (25), and (26),

$$\left| F(a,b;c;-z) \right| \leq A' \frac{\Gamma(c)}{\Gamma(a)\Gamma(b)} \; \frac{\Gamma(a+b-c)}{\pi^{a+b-c}} \, . \tag{27}$$

Parameters a, b, and c, and also z are assumed real and positive.

The series for $I(x,\rho;u)$ has been shown to converge for $u < |x-\rho|$, $\rho < x$. Utilization of Equations (27) and (17) yield the results

$$\left| I(x,\rho;u) \right| \leq A' \frac{\rho u}{x^2} \sum_{m=0}^{\infty} \frac{\Gamma(2m+1/2)}{m!\,(m+1)!} \left| \frac{\rho}{\pi x} \right|^{2m} \tag{28}$$

so Equation (17) converges over the extended range $\rho < (\pi/2)x$, $u < x$. A transformation of the hypergeometric function (Ref. 22, page 64) yields

$$F\left\{ m+1/2, m+3/2; 3/2; -\left(\frac{u}{x}\right)^2 \right\} = \left(\frac{x^2}{x^2+u^2}\right)^{m+1/2} F\left\{ m+1/2, -m, 3/2; \frac{u^2}{x^2+u^2} \right\}, \tag{29}$$

where the hypergeometric function on the right is a polynominal defined for all x and u. Since u and x are real, z is real in Equations (25) and (27); it follows that these relations are valid for all $z \geq 0$ provided F is defined for $z > 1$ in Equation (27). But the hypergeometric function in Equation (17) is defined for all u and x by Equation (29) and hence, according to Equation (28) and the foregoing discussion, Equation (17) converges for all values of u and x for $\rho < (\pi/2)x$. Consequently,

$$I(x,\rho;u) = 2 \frac{u}{x} \sum_{m=0}^{\infty} \frac{\Gamma(m+1/2)\Gamma(m+3/2)}{m!\,(m+1)!} \left| \frac{\rho^2}{x^2+u^2} \right|^{m+1/2} F\left\{ m+1/2, -m; 3/2; \frac{u^2}{x^2+u^2} \right\} \tag{30}$$

for $\rho < (\pi/2)x$ by analytic continuation. An expression valid for $x < (\pi/2)\rho$ can be obtained by interchanging ρ and x in the right hand member of this equation.

37

An expression for $G(x,u)$ can be obtained upon substitution of Equation (30) into Equation (9); interchange of summation and integration is permissible since evidently Equation (30) is uniformly convergent on $a < \rho \leqslant b$ provided $x > (2/\pi)b$. Hence,

$$G(x,u) =$$

$$2\,\frac{u}{x} \sum_{m=0}^{\infty} \frac{\Gamma(m+1/2)\Gamma(m+3/2)}{m!(m+1)!(2m+3)}\; \frac{b^{2m+3} - a^{2m+3}}{(x^2+u^2)^{m+1/2}}\; F\left\{m+1/2,-m;3/2;\;\frac{u^2}{x^2+u^2}\right\}\quad (31)$$

for $x > (2/\pi)b$. An expression valid for $x < (\pi/2)a$ can be derived by interchanging ρ and x in the right side of Equation (30);

$$G(x,u) =$$

$$2 \sum_{m=0}^{\infty} \frac{\Gamma(m+1/2)\Gamma(m+3/2)}{m!(m+1)!}\; u^2\left(\frac{x}{u}\right)^{2m+1} \int_{a}^{b}\left(\frac{u^2}{\rho^2+u^2}\right)^{m+1/2} F\left\{m+1/2,-m;3/2;\frac{u^2}{\rho^2+u^2}\right\}\frac{d\rho}{u}, \quad (32)$$

The substitution $\rho = u\,\tan\emptyset$ leads to

$$G(x,u) = 2u^2 \sum_{m=0}^{\infty} \frac{\Gamma(m+1/2)\Gamma(m+3/2)}{m!(m+1)!}\left(\frac{x}{u}\right)^{2m+1} V_m(u;a,b) \quad (33)$$

where

$$V_m(u;a,b) = \sum_{n=0}^{m} (-)^n \binom{m}{n} \frac{(m+1/2)_n}{(3/2)_n}\; Y_{m+n}\,(u;a,b) \quad (34)$$

with

$$Y_n = \int_{\emptyset(a)}^{\emptyset(b)} \cos^{2n-1}\theta\, d\theta \quad (35)$$

Hence,

$$Y_o = \ln \frac{b + \sqrt{b^2+u^2}}{a + \sqrt{a^2+u^2}} \quad (36)$$

38

and $Y_1, Y_2, \ldots$ can be obtained in succession from

$$Y_{n+1} = \frac{1}{2n+1}\left[\frac{b}{\sqrt{b^2+u^2}}\left(\frac{u^2}{b^2+u^2}\right)^n - \frac{a}{\sqrt{a^2+u^2}}\left(\frac{u^2}{a^2+u^2}\right)^n\right] + \frac{2n}{2n+1}Y_n \qquad (37)$$

Thus, for $x < (\pi/2)a$, $G(x,u)$ is defined by Equations (33), (34), (36), and (37).

If $(2/\pi)b < (\pi/2)a$, $G(x,u)$ is defined for the entire range of x and u. If not, an expression is needed in the gap $(\pi/2)a < x < (2/\pi)b$. Accordingly, Equation (9) can be written

$$G(x,u) = \int_a^x \rho\, I(x,\rho;u)d\rho + \int_x^b \rho\, I(x,\rho;u)d\rho \qquad (38)$$

The first integral can be evaluated in the same manner as Equation (31) and the second in the same manner of Equation (33). Hence,

$$G(x,u) = 2\,\frac{u}{x}\sum_{m=0}^{\infty}\frac{\Gamma(m+1/2)\Gamma(m+3/2)}{m!(m+1)!(2m+3)}\frac{x^{2m+3}-a^{2m+3}}{(x^2+u^2)^{m+1/2}}F\left\{m+1/2, -m; 3/2; \frac{u^2}{x^2+u^2}\right\}$$

$$+ 2u^2\sum_{m=0}^{\infty}\frac{\Gamma(m+1/2)\Gamma(m+3/2)}{m!(m+1)!}\left(\frac{x}{u}\right)^{2m+1}V_m(u;x,b) \qquad (39)$$

The first summation is obtained by substituting x for b in Equation (31) and the second by substituting x for a in Equations (33), (34), (36), and (37). Equation (39) is valid for $(2/\pi)a < x < (\pi/2)b$. It is seen there is an overlap in the regions of validity of the three expressions for $G(x,u)$.

The derivation for the magnetic vector potential is complete, and is given by Equations (2), (6), (31), (33), and (39), along with

Equations (34), (36), and (37). To obtain $\vec{A}$ at points other than in the X-Z plane, it is only necessary to replace x with $\rho = \sqrt{x^2+y^2}$, and replace 1_y with $(-1_x y + 1_y x)/\rho$, where 1_x and 1_y are unit vectors. Thus

$$\vec{A}(x,y,z) = \frac{-1_x y + 1_y x}{\sqrt{x^2+y^2}} A(\sqrt{x^2+y^2}, z) = 1_\phi A(\rho,z) \tag{40}$$

The magnetic field is obtained from the vector potential from the relations

$$\vec{B} = \nabla \times \vec{A} \tag{41}$$

In the example of interest

$$B_\rho = -\frac{\partial A}{\partial z} \tag{42}$$

$$B_\phi = 0 \tag{43}$$

$$B_z = \frac{1}{\rho} \frac{\partial}{\partial \rho} (\rho A) \tag{44}$$

where B_ρ and B_z are directed along ρ and z, respectively. B_ϕ is the component in the X-Y plane normal to ρ (i.e., B_ϕ is directed along 1_ϕ). Using the previous notation for consistency, ρ is replaced by x in the Equation for $\vec{B}$ in the following analysis; x can be replaced by ρ in the final equations. Thus, according to Equations (6), (7) and Equations (42) through (44)

$$B_x = -\frac{\mu_o j}{4\pi}\left[\frac{\partial}{\partial z} G(x,z-h) - \frac{\partial}{\partial z} G(x,z-k)\right] = -\frac{\mu_o j}{4\pi}\left[G_z(x,z-h) - G_z(x,z-k)\right] \tag{45}$$

where

$$G_z(x,z-\zeta) = \frac{\partial G(x,u)}{\partial u}\Bigg|_{u=z-\zeta} \tag{46}$$

40

with ζ = k or h. Also,

$$B_y = 0 \tag{47}$$

and

$$B_z = \frac{\mu_0 J}{4\pi}\left[\frac{1}{x}\frac{\partial}{\partial x}\left\{xG(x,z-h)\right\} - \frac{1}{x}\frac{\partial}{\partial x}\left\{xG(x,z-k)\right\}\right]$$

$$= \frac{\mu_0 J}{4x}\left[G_x(x,z-h) - G_x(x,z-k)\right] \tag{48}$$

when

$$G_x(x,z-\zeta) = \frac{1}{x}\frac{\partial}{\partial x}\left\{xG(x,u)\right\}\Bigg|_{u=z-\zeta} \tag{49}$$

The analysis will be complete when expressions for

$$\frac{\partial G(x,u)}{\partial u} = G_u(x,u) \tag{50}$$

and

$$\frac{1}{x}\frac{\partial}{\partial x}\left\{xG(x,u)\right\} = G_x(x,u) \tag{51}$$

have been derived.

From Equation (31), one obtains

$$G_u(x,u) = 2x\sum_{m=0}^{\infty}\frac{\Gamma(m+1/2)\Gamma(m+3/2)}{m!(m+1)!(2m+3)}\frac{b^{2m+3}-a^{2m+3}}{(x^2+u^2)^{m+3/2}} F\left\{m+3/2,-m;1/2;\frac{u^2}{x^2+u^2}\right\} \tag{52}$$

and

$$G_x(x,u) = -4u\sum_{m=0}^{\infty}\frac{\left[\Gamma(m+3/2)\right]^2}{m!(m+1)!(2m+3)}\frac{b^{2m+3}-a^{2m+3}}{(x^2+u^2)^{m+3/2}} F\left\{m+3/2;-m;3/2;\frac{u^2}{x^2+u^2}\right\} \tag{53}$$

for $x > (2/\pi)b$. As can be shown from Equations (32) and (33),

$$G_u(x,u) = 2\sum_{m=0}^{\infty}\frac{\Gamma(m+1/2)\Gamma(m+3/2)}{m!(m+1)!}\left(\frac{x}{u}\right)^{2m+1}\left[-(2m-1)uV_m(u;a,b)\right.$$

$$\left. + a\left(\frac{u^2}{a^2+u^2}\right)^m F\left\{m+1/2,-m;3/2;\frac{u^2}{a^2+u^2}\right\}\right.$$

41

$$- b \left(\frac{u^2}{b^2+u^2} \right)^m F\left\{ m+1/2, -m; 3/2; \frac{u^2}{b^2+u^2} \right\} \Bigg]$$ (54)

and

$$G_x(x,u) = 4u \sum_{m=0}^{\infty} \frac{\Gamma(m+1/2)\Gamma(m+3/2)}{\left[m! \right]^2} \left(\frac{x}{u} \right)^{2m} V_m(u;a,b)$$ (55)

for $x < (\pi/2)a$. Examination of Equations (38) and (39) shows that the expression for $G_u(x,y)$ valid on $(2/\pi)a < x < (\pi/2)b$ can be obtained by substituting x for b in Equation (52), x for a in Equation (54), and adding the two resultant expressions. An expression can be obtained in a similar manner for $G_x(x,y)$ from Equations (53) and (55), as examination of Equation (38) shows. Derivatives with respect to the limits of integration in Equation (38) cancel.

42

REFERENCES

1. Wilson, R. K., Miller, R. A., and Kloster, R. L., A Study of Space Radiation Shielding Problems for Manned Vehicles. General Dynamics/Fort Worth Report FZK-144, 8 June 1963.

2. Norwood, J. M., The Combination of Active and Passive Shielding. General Dynamics/Fort Worth Report FZM-2754, paper presented at the Symposium on the Protection Against Radiation Hazards in Space, Gatlinberg, Tennessee, 5-7 November 1962 (and other unpublished work).

3. Dow, N. F., Shen, S. P. and Heyda, J. F., Evaluations of Space Vehicle Shielding. General Electric, Space Sciences Laboratory, R62SD31, April 1962.

4. Levy, R. H., Radiation Shielding of Space Vehicles by Means of Superconducting Coils. Avco-Everett Research Laboratroy, Research Report 106, AFBSD-TN-61-7, April 1961.

5. Stormer, C., The Polar Aurora. Oxford, 1955; Janossy, L., Cosmic Rays. Oxford, 1950; for recent related work, see MacLeod, M. A., and Waniek, R. W., 'Injection of High Velocity Charged Particles into Strong Magnetic Fields," Journal of Applied Physics, 34, 1415 (1963).

6. Tooper, R. W., and Davies, W. O., Electromagnetic Shielding of Space Vehicles. Armour Research Foundation, IAS Paper No. 62-156, presented at the IAS National Summer Meeting, Los Angeles, California, June 19-22, 1962.

7. Swann, W. F. G., "Application of Liouville's Theorem to Electron Orbits in the Earth's Magnetic Field," Physical Review, 44, 224 (1933).

8. Tooper, R. F., Electromagnetic Shielding Feasibility Study. Armour Research Foundation, ASD-TRD-63-194, May 1963.

9. Hulm, J. K., et al., "Superconducting Magnets," International Science and Technology, May 1963, p. 55.

10. Autler, S. H., "Superconducting Magnets,' High Magnetic Fields, edited by H. Kohm, et al. Published jointly by the M.I.T. Press and John Wiley and Sons, Inc. New York, 1962.

11. Betterton, J. O., Jr., et al., Size Effects and Interstitial Impurities in Nb3-Zr Superconductors. Superconducting Solenoids with Metal Insulation, Oak Ridge National Laboratory Report 3303 (1962).

12. Montgomery, D. B., _Current-Carrying Capacity of Nb-Zr Solenoids_, National Magnet Laboratory Report AFOSR-3015, July 1962.

13. Boom, R. W., et al., "Superconducting Magnet Development," _Electronuclear Division Annual Progress Report for Period Ending December 13, 1962_, Oak Ridge National Laboratory Report 3432.

14. Boom, R. W., and Livingston, R. W., "Superconducting Solenoids," _Proceedings of the IRE_, 50, 274 (1962).

15. Germain, C., "Review of Methods of Measuring Magnetic Fields," _Nuclear Instruments and Methods_, 21, 26 (1963).

16. Olsen, J. L., and Rinderer, L., "Magneto-Resistance of Copper up to 150,000 Oersted at 4.2°K," _Nature_, 173, 682 (1954).

17. Cotti, P., "Size Effects in Magnetic Fields," _High Magnetic Fields_, edited by H. Kolm, et al. Published jointly by the M.I.T. Press and John Wiley and Sons, Inc., New York, 1962.

18. Ollard, E. A., and Smith, E. B., _Handbook of Industrial Electroplating_, Illife and Sons, Ltd., London, 1958, p. 136.

19. Graham, A. K., _Electroplating Engineering Handbook_, Reinhold Publishing Corp., New York, 1962, p. 206.

20. Laquer, H. L., "An Electrical Flux Pump for Superconducting Magnet Coils," _Cryogenics_, 3, 27 (1963).

21. Smith, P. F., "Protection of Superconducting Coils." _Review of Scientific Instruments_, 34, 368 (1963).

22. Bateman, H., _Higher Transcendental Functions_, McGraw-Hill, New York, 1953.